01

The Structure of low-lying electromic states of the polar Rb2Cs trimer based on ab initio calculations

© *E.A. Bormotova*[1], *A.S. Likharev*[1], *K.E. Kopylov*[2,3], *V.V. Krotov*[2,3], *S.V. Kozlov*[1], *A.V. Stolyarov*[1]

[1] Department of Chemistry, Moscow State University,
Moscow, Russia
[2] University Gymnasium, Lomonosov Moscow State University,
Moscow, Russia
[3] Research Computing Center, Lomonosov Moscow State University,
Moscow, Russia

e-mail: bormotova.e.a@gmail.com, avstol@gmail.com

Received May 05, 2024
Revised June 25, 2024
Accepted June 29, 2024

Ab initio quantum chemical calculations of the electronic structure of the ground and low-lying doublet and quartet states of the Rb_2Cs molecule were performed, as a result of which 3D potential energy* [1] surfaces (PES) were obtained simulating the approach of a Rb atom towards a RbCs dimer aimed at bothe the Cs atom and the Rb atom at different angles of attack varying in the range from 10° to 180°. It is shown that the ground state of the heteronuclear trimer $(1)^2A'$ exhibits an avoided crossong with the first excited $(2)^2A'$ state near the equilibrium geometry, therefore the ground state of Rb_2Cs cannot be described within the framework of the traditional adiabatic approximation. For all 12 electronic states studied, equilibrium parameters corresponding to the C_{2v} point group were determined. The constructed PES can be used for quantum calculation of collision cross sections and rate constants for the reaction of an RbCs dimer with a Rb atom, as well as conducting detailed analyses of the rovibronic structure of the trimer by solving the 3D vibrational-rotational Schrödinger equation in order to find optimal ways for laser synthesis, cooling and manipulation of the ultracold ensemble of this atomic-molecular system.

Keywords: quantum chemical calculations, electromic structure, potential energy surfaces, heteronuclear trimers, alkali metals, ultracold molecules.

DOI: 10.61011/EOS.2024.07.59642.6426-24

1. Introduction

Creating the most effective optical paths for the direct synthesis of stable polar molecular ensembles with ultralow translation and internal temperature is of key importance for the further development of several fundamental and applied fields of molecular physics and physical chemistry beginning from laser-induced chemical reactions controlled by an external electromagnetic field with reagents at submicron temperatures [1–3] to ultraprecision metrological measurements and the creation of hardware components (qubits) for quantum computers [4–7].

Laser assembly and the spatial confinement of ultracold atomic-molecular-level ensembles, with high spatial particle density, are known to be complicated by a considerable dissipation of energy induced by elastic and inelastic collisions between individual atoms and the molecules they form [8]. Therefore, extensive experimental and theoretical studies are currently underway to reduce self-induced dissipative (collisional) energy loss as much as possible [9,10] to increase laser synthesis efficiency.

The focus of fundamental studies of ultracold molecules has shifted accordingly over recent years from di-atomic [11] to tri-atomic [12] systems. Thus, numerous theoretical and experimental studies have emerged addressing homonuclear trimers such as Rb_3, K_3 and Na_3 [13,14]. Studies gradually begin to emerge addressing A_2B type heteronuclear molecules where a heteronuclear dimer, AB, collides with its constituent atom, A (molecules of this type can be, for example, formed during laser assembly of alkali metal dimers) [15–20]. In particular, there are several quantum chemical studies addressing three-atom systems consisting of rubidium and cesium: [20–22] addressed only lower doublet and quartet states, [23] addressed the asymptotic behavior of potential energy surfaces (PES) at large internuclear distances, [23] simulated reactions between two dimers, and the experimental study [8] addressed collisional loss rates in reactions between RbCs dimers and constituent Rb and Cs atoms.

2. Equilibrium geometries of the ground and excited states of the Rb_2Cs molecule

Similar to previous calculations [24–27], quantum-chemical calculations have been conducted in this work using effective core potentials (ECP) for the Rb and

* [1] Tabulated numerical results are available on request: *bormotova.e.a@gmail.com*.

Table 1. Energetic minimums of low-lying doublet and quartet states of the Rb_2Cs molecule. The distance between atoms A and B $R_{\text{A-B}}$ and the angle at the Cs atom θ_{Cs} are given in Å and degrees, respectively. Energy is given in cm^{-1} with respect to the energy minimum in the electronic ground state $(1)^2\text{A}'$

State	$R_{\text{Rb-Cs}}$, Å	$R_{\text{Rb-Rb}}$, Å	θ_{Cs}, deg	E_{min}, cm^{-1}
$(1)^2\text{A}'$	4.54	5.23	70	0
$(2)^2\text{A}'$	4.81	4.43	55	602
$(3)^2\text{A}'$	4.56	5.94	81	5966
$(4)^2\text{A}'$	5.07	4.81	57	7109
$(5)^2\text{A}'$	4.80	4.41	55	7793
$(6)^2\text{A}'$	4.76	5.24	67	11348
$(1)^2\text{A}''$	4.46	4.22	56	4546
$(2)^2\text{A}''$	4.45	4.91	67	9596
$(1)^4\text{A}'$	5.47	5.29	58	4794
$(2)^4\text{A}'$	4.60	7.73	114	9549
$(3)^4\text{A}'$	4.58	9.15	180	11867
$(1)^4\text{A}''$	4.51	5.35	73	8861

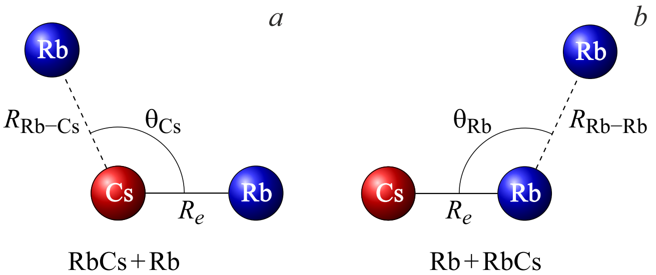

Figure 1. Geometries corresponding to the Rb atom approaching the RbCs dimer (*a*) in direction of the Cs atom (*b*) and in the direction of the the Rb atom.

Cs atoms using the Stuttgart basis sets ECP28MDF and ECP46MDF, respectively [28]. These basis sets consist of uncontracted Gaussian basis functions [13s9p5d3f1g] and [12s11p5d3f2g], respectively, and they leave 9 electrons each (1 valence and 8 subvalence electrons) to explicitly account for electron correlation. Core-valence correlation effects were considered using the Müller–Meyer type model core-polarization potential (CPP) [29]. CPP parameters were selected in [24,30] in such a way as to reproduce the first dissociation limits of the molecule corresponding to the atomic transitions $\text{Rb}(5s)\to\text{Rb}(5p)$ $12737.34\,\text{cm}^{-1}$ and $\text{Cs}(6s)\to\text{Cs}(6p)$ $11547.63\,\text{cm}^{-1}$ [31]. Static dipole polarizabilities necessary for the CPP parameterization were assumed equal to 9.096 and 15.687 a.u. for the singly charged Rb^+ and Cs^+ , respectively, and cut-off radii are 0.373 and 0.2697 a.u.

During the optimization of the molecular orbitals (MO) using the complete active space self-consistent field (CASSCF) method with spin averaging, all electrons in the subvalence shells remained in 12 doubly occupied MOs: 9 MOs belonging to the symmetry group A′ and 3 MOs belonging to the symmetry group A″. Three valence

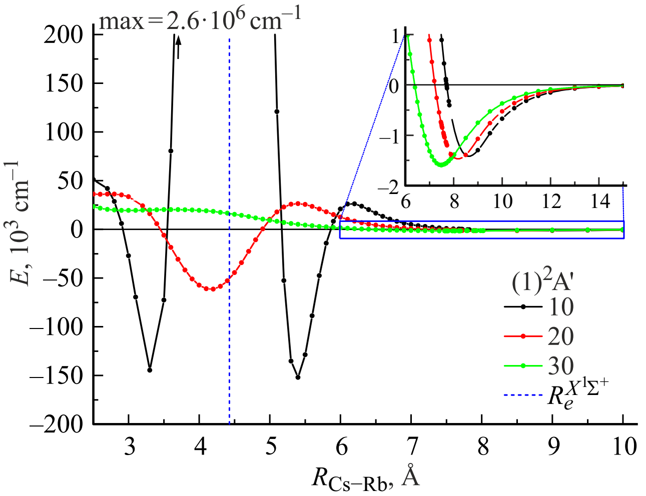

Figure 2. Cross-sections of PES for RbCs + Rb corresponding to the $(2)^2\text{A}'$ state of the Rb_2Cs trimer obtained at fixed distances between the first Rb atom and the Cs atom ($R_e^{X^1\Sigma^+}(\text{RbCs}) = 4.427$ Å). Each curve corresponds to the incidence angle of $\text{Rb}\theta_{\text{Cs}} = 10°$, 20°, 30° at the Cs atom. The cross-sections are shown as functions of the distances between the incident Rb atom and the Cs atom, $R_{\text{Cs-Rb}}$. The vertical dashed blue line marks the distance at which $R_{\text{Cs-Rb}} = R_e^{X^1\Sigma^+}$.

electrons of the Rb_2Cs molecule remained available for excitation to higher MOs. The active space consisted of 16/4 MOs belonging to the A′/A″ symmetries (this slash designation is used hereafter for orbitals belonging to the two symmetry groups in this order). Dynamic correlation effects were accounted for only for the three remaining valence electrons of the molecule using the multireference configuration interaction method with single and double excitations (*ic*-MR-CISD).

The search for the equilibrium geometries of the ground and excited states converging to the first dissociation limit was conducted in several stages. First, coarse-grid ($\Delta R = 0.5$ Å) computations were conducted, where all three interatomic distances varied within (3–10) Å. Almost all local minima occurred at geometries where all three internuclear distances fall within (4.5–6) Å. Then the grid was condensed 5 fold up to a step of $\Delta R = 0.1$ Å. As a result, it was found that, for the studied states, potential minima are observed on the PES for geometries where the distances between the Cs atom and both Rb atoms either coincide or differ by the minimum step used for the grid. Therefore it was concluded that that the equilibrium geometry of all studied states belonged to the C_{2v} point group. For all studied states, the geometry was optimized using the MOLPRO program package [32] using the quadratic steepest descent method. Optimization was performed using the initial geometry of an symmetric isosceles triangle by varying two parameters: the internuclear distance between the Cs atom and Rb atoms and angle on the Cs atom. To ensure that the optimized geometry actually corresponds to any equilibrium, several analogous computations were performed for each state by choosing a different starting

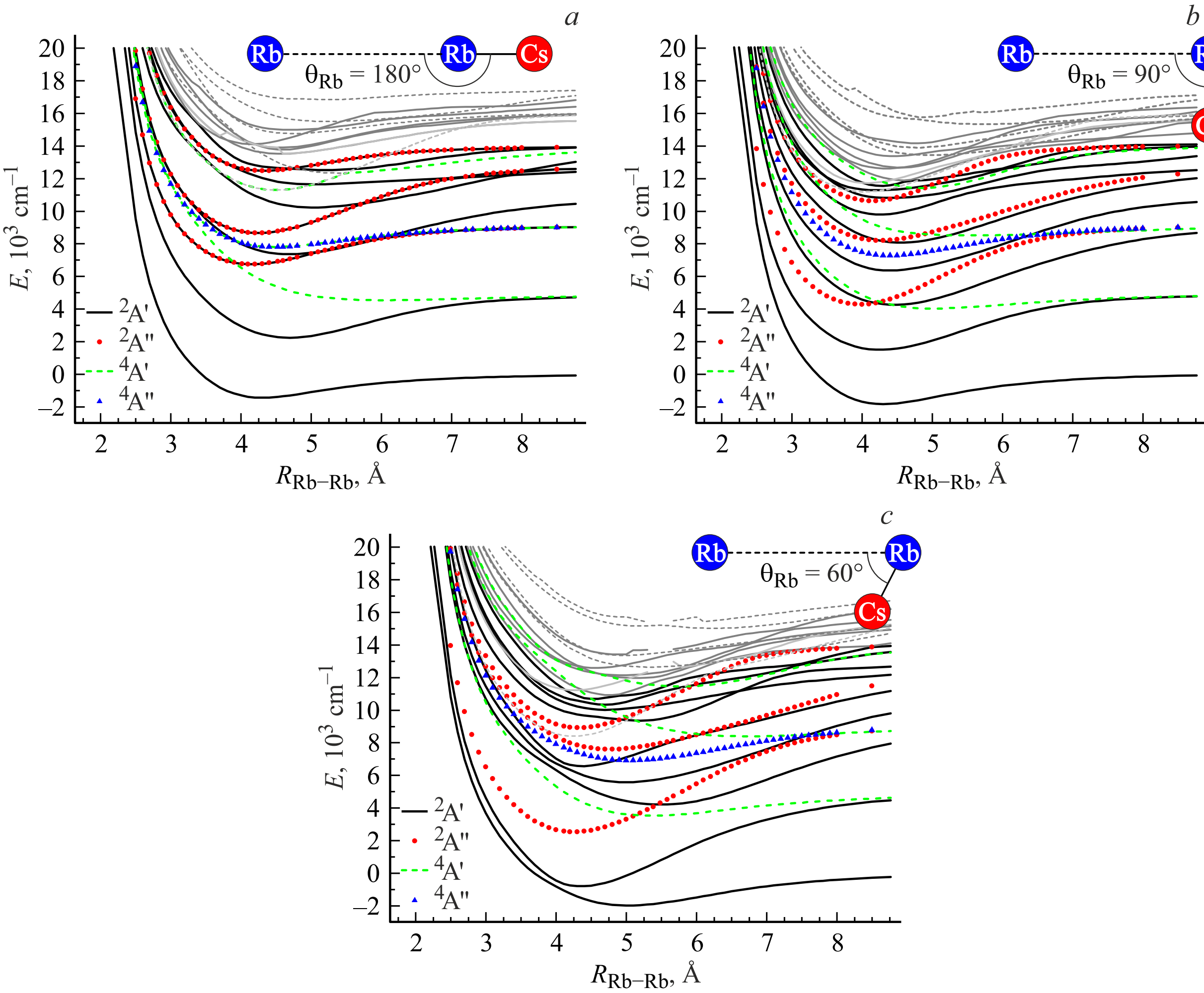

Figure 3. PES cross-section for Rb+RbCs at the fixed distance in the RbCs dimer $R_e^{X^1\Sigma^+} = 4.427$ Å as function of the distance between the incident Rb atom and the Rb atom in the $R_{\text{Rb-Rb}}$ dimer at the incidence angles (*a*) $\theta_{\text{Rb}} = 180^\circ$, (*b*) $\theta_{\text{Rb}} = 90^\circ$, (*c*) $\theta_{\text{Rb}} = 60^\circ$.

geometry far from the equilibrium one (for example, by increasing the distance $R_{\text{Cs-Rb}}$ from 4.1 to 7 Å) as the initial geometry. All computations performed for identical states converged to the same equilibrium parameters. For additional verification, the optimized parameters belonging to the symmetry group C_{2v} were used as the parameters for the initial geometry, but the geometry optimization was performed for three geometrical parameters (the symmetry group reduced to the C_s symmetry at program-level). This procedure allows for the distances between the Cs and two Rb atoms to differ from each other, if such geometry was really more favorable — however, this was not the case. The final results are shown in Table 1.

For almost all studied states, the equilibrium internuclear distances remain within the distances typical of the alkali metal atom bonds (i.e. within 4–6 Å). For all states, the isosceles triangle geometry (where the distances between the Cs atom and each of the Rb atoms are identical) appeared to be the most energetically favorable, moreover, for most states, the optimal geometry is close to the isosceles triangle geometry. Thus, for example, seven states have equilibrium geometry angles deviating from 60° by less than 7°. However, most states (also 7 of 12) the exhibited equilibrium distances between the Rb atoms and Cs atom remains within 4.5 ± 0.1 Å. This aspect might be critically important, because the ground state of the RbCs dimer has an equilibrium distance of 4.427 Å, which is conducive to the formation of Rb_2Cs trimers when Rb atoms collide with ground state dimers. Note that two states can be highlighted among the examined states: the $(3)^4\text{Å}'$ state — as the only state with a linear equilibrium geometry, and the $(2)^4\text{A}'$ state, for which the angle on the Cs atom is 114.49°. The optimum geometry of the $(1)^2\text{Å}'$ ground state has been already addressed in [22], where the same isosceles triangle geometry belonging to the symmetry group C_{2v} with $R_{\text{Rb-Rb}} = 5.5$ Å and $R_{\text{Rb-Cs}} = 4.6$ Å, which corresponds to $\theta_{\text{Cs}} = 73.4^\circ$, was the optimum one. The authors of [22] had determined that the atomization energy (i.e. the energy needed to break all bonds) was equal to 5781 cm^{-1}. These results agree quite well with the present data (Table 1). The only deviation, of 0.3 cm, can be seen in the $R_{\text{Rb-Rb}}$ state. To compare these results, the well

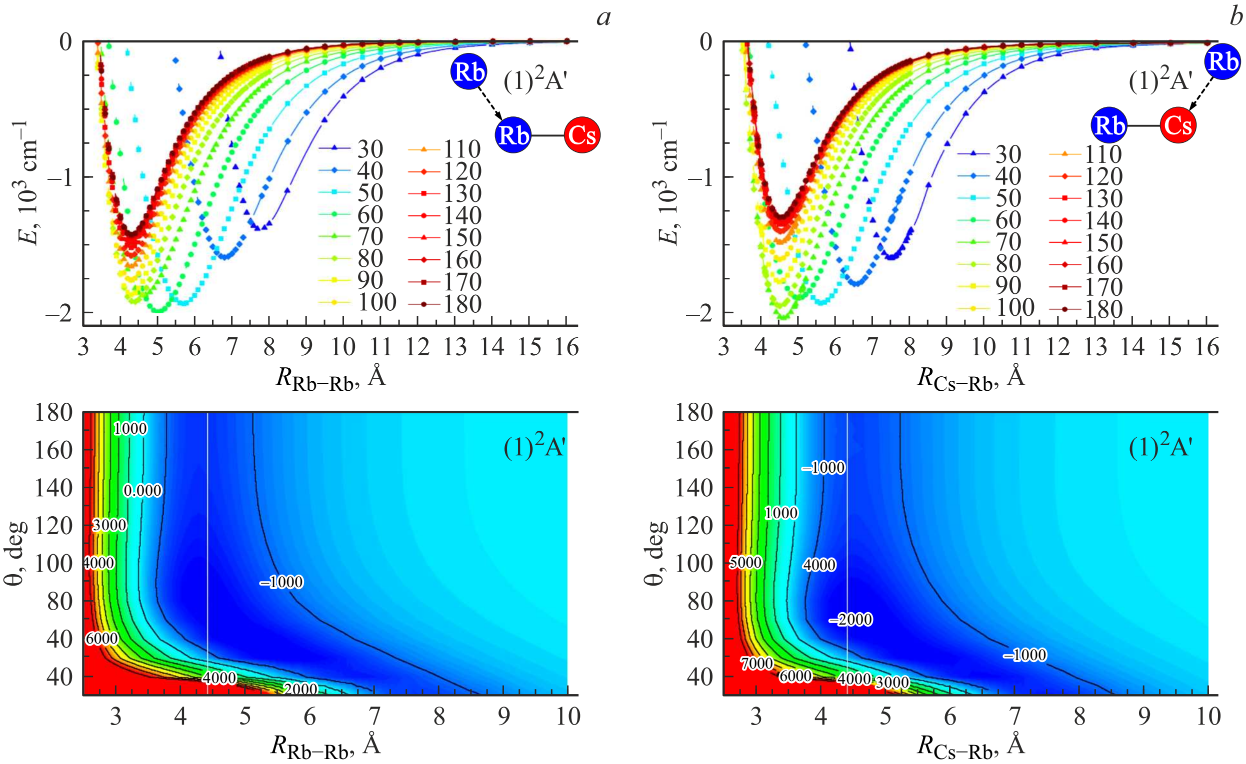

Figure 4. PES (bottom) and their cross-sections (top) at different incidence angles for the ground state $(1)^2A'$ in the case of (a) Rb+RbCs and (b) RbCs+Rb. The values were obtained at $R_e^{X^1\Sigma^+} = 4.427$ Å. The vertical white lines in the diagrams on the bottom correspond to positions where the distance between the incident and attacked atoms is equal to R_e. Each outline corresponds to a step of $1000\,\mathrm{cm}^{-1}$.

depth of the ground state with respect to the dissociation limit for RbCs($X^1\Sigma^+$)+Rb($5s$) can be used, which in the present work is equal to $2053\,\mathrm{cm}^{-1}$ and to this add the dissociation energy for the RbCs dimer ($3845\,\mathrm{cm}^{-1}$ [33]). Thus, one obtains 5898 cm, which differs from the value obtained in [22] by less than 2%. In [20], for the $(1)^4A'$ quartet ground state, the equilibrium geometry was equal to 5.46 Å and 58°, which agrees perfectly with the results obtained in this study — (5.469 Å, 57.82°).

3. Potential energy surfaces of the convergence of the Rb atom and RbCs dimer

Since the main interest in alkali metal trimers is attributable to the fact that unwanted loss of molecules is observed during the laser assembly process, and one of the possible mechanisms behind this loss being collisions between the dimer and a free alkali metal atom, spatial scanning of the PES was performed in this work primarily in a way that simulates these collisions. Thus, two cases, shown in Figure 1, were addressed. Case (a) is the attack by the free Rb atom of the RbCs dimer's constituent Cs atom (designated hereafter as RbCs+Rb). Case (b) is the attack by the free Rb atom of the RbCs dimer's constituent Rb atom (designated hereafter as Rb+RbCs).

In both cases, the internuclear distance in the R_e dimer is fixed and corresponds to one of four values $R_e^{X^1\Sigma^+} = 4.427$ Å, $R_e^{a^3\Sigma^+} = 6.219$ Å, $R_e^{A^1\Sigma^+} = 5.122$ Å or $R_e^{b^3\Pi} = 4.314$ Å that are equal to the equilibrium positions of the corresponding electron states of the RbCs dimer. Then, calculations were conducted at different incidence angles $\theta \in [30°, 180°]$ at 10° intervals and at different distances $R_{\text{Rb-A}}$ between the incident Rb atom and attacked A = Rb, Cs atom in the dimer. R_e values were chosen according to the potential curves plotted earlier for the RbCs dimer: the chosen distances correspond to the minimum energy positions on the potential curves of the RbCs dimer in the ground state ($X^1\Sigma^+$) and three lowest excited states $a^3\Sigma^+$, $A^1\Sigma^+$, $b^3\Pi$. The corresponding quantum chemical calculations of the dimers were carried out using a scheme identical to the trimer calculation scheme. However, these calculations used larger atomic basis sets [30], and the active space consisted of the first 10/5/5/2 MOs corresponding to the $a_1/b_1/b_2/a_2$ symmetries. All sixteen subvalence electrons remained on the doubly occupied 4/2/2/0 orbitals. Cut-off parameters for the CPP potentials were taken to be equal to 0.392 and 0.2765 a.u. for the Rb^+ and Cs^+ cations, respectively.

Let's first consider the behavior of the approach PES of the Rb atom and the RbCs dimer at small angles in 10°, 20° and 30° as shown in Figure 2 for the first doublet state A' when the attacking Rb atom approaches the Cs atom. At

Table 2. The spectroscopic constants $R^{\mathrm{A}}_{\min}$ (Å), D^{A}_{e} (cm^{-1}) for the triatomic $\mathrm{Rb_2Cs}$ system at some incidence angles $\theta^{\mathrm{A}}_{\min}$ of A = Rb, Cs in the RbCs dimer attacked by the third Rb atom. T_e is the value of the PES at the dissociation limit corresponding to the Rb+RbCs or RbCs+Rb system with a constant internuclear distance R_e in the RbCs dimer. The chosen incidence angles correspond either to the minimum value on the PES or to a saddle point with respect to the incidence angle (marked with $*$)

$R_e^{X^1\Sigma^+} = 4.427$ Å															
State	T_e, cm^{-1}	$\theta^{\mathrm{Rb}}_{\min}$, deg	$R^{\mathrm{Rb}}_{\min}$, Å	D^{Rb}_{e}, cm^{-1}	$\theta^{\mathrm{Cs}}_{\min}$, deg	$R^{\mathrm{Cs}}_{\min}$, Å	D^{Cs}_{e}, cm^{-1}	State	T_e, cm^{-1}	$\theta^{\mathrm{Rb}}_{\min}$, deg	$R^{\mathrm{Rb}}_{\min}$, Å	D^{Rb}_{e}, cm^{-1}	$\theta^{\mathrm{Cs}}_{\min}$, deg	$R^{\mathrm{Cs}}_{\min}$, Å	D^{Cs}_{e}, cm^{-1}
$(1)^2\mathrm{A}'$	0	60	5.01	1998	50	5.63	1924	$(1)^2\mathrm{A}''$	9094	60	4.26	6579	60	4.38	6537
		70*	4.63	1876	60*	5.00	1886			180*	4.15	2345	180*	4.35	1860
		80	4.39	1924	70	4.59	2035	$(2)^2\mathrm{A}''$	12743	60	4.78	5166	70	4.41	5187
		180*	4.31	1430	180*	4.53	1294			180*	4.25	4077	130*	4.43	4421
$(2)^2\mathrm{A}'$	4861	40*	7.38	2435	30*	8.00	2465						180	4.43	4470
		60	4.35	5678	60	4.60	5737	$(1)^4\mathrm{A}'$	4862	70	5.04	1424	60	5.35	1424
		120*	4.69	2455	100*	4.88	2435			180*	6.07	314	180*	6.21	320
		180	4.70	2613	180	4.85	2694	$(2)^4\mathrm{A}'$	9086	30	7.88	1548	30	7.92	1231
$(3)^2\mathrm{A}'$	9085	50	5.93	5149	50	6.06	6644			80*	6.38	516	70*	6.63	530
		70*	5.11	4655	60*	5.53	6481			150	4.50	1321	120	4.64	1555
		90	4.48	4870	80	4.63	6967			180*	4.49	1280	180*	4.75	1050
		180*	4.16	2340	180*	4.35	3678	$(3)^4\mathrm{A}'$	14057	70*	5.09	2620	70*	5.24	2610
$(4)^2\mathrm{A}'$	10903	70	4.62	5428	60	5.02	5471			120	4.76	2778	180	4.53	4208
		130*	4.70	3067	130*	4.97	2843			160*	4.55	2754			
		180	4.70	3528	180	5.09	3209			170	4.51	2756			
$(5)^2\mathrm{A}'$	12736	40*	7.27	4295	40*	6.98	4659			180*	4.50	2754			
		60	4.38	6186	60	4.65	6321	$(1)^4\mathrm{A}''$	9094	30*	7.82	1457	70	4.54	2268
		100*	4.59	4645	100*	4.79	4286			50	5.69	2217	180*	4.76	1055
		120	4.51	4766	130	4.68	4468			180*	4.50	1287			
		180*	4.26	4073	180*	4.43	4460								
$(6)^2\mathrm{A}'$	12746	40*	7.74	1406	30*	8.39	1548								
		70	4.85	3550	60	5.28	3534								
		120*	4.82	1500	100*	4.91	1399								
		180	5.03	2519	180	5.34	2341								

such incidence angles, the attacking atom and the second (not attacked) dimer atom pass by each other at extremely short distances when $R_{\text{Cs-Rb}}$ (or $R_{\text{Rb-Rb}}$) is approximately equal to the internuclear distance R_e in the dimer. Thus, at the incidence angles of 10°, 20° and 30°, the Rb atoms come within distances of 0.772, 1.537 and 2.292 Å, up to the second dimer atom, which is much lower than the internuclear distances typical of the ground state and excited states of $\mathrm{Rb_2}$, that are approximately within 3.5–5.5 Å [34].

The PES corresponding to the incidence angle of 10° has several features. As expected, a very high peak (2.60479×10^6 cm^{-1}) is observed at $R_{\text{Cs-Rb}} \approx R_e^{X^1\Sigma^+}$. However, there are also two deep minima — one at 3.3 and the other at 5.4 Å. Despite the significant great depth of these minima (-140.75×10^6 and -150.9×10^6 cm^{-1}), these configurations will be achievable only in the case of very high collision energies, because, when the atoms approach the dimer from infinity, the $\mathrm{Rb_2Cs}$ molecule passes the stable configuration $R_{\text{Cs-Rb}} = 8.7$ Å and $R_{\text{Rb-Rb}} = 4.4$ Å, which is typical of the valence bond lengths between two alkali metal atoms. To exit this geometry by decreasing the distance between the attacking Rb atom and the farther atom in the dimer, a potential barrier of $26.2 \cdot 10^3$ cm^{-1} must be overcome first.

An interesting behavior is also observed for the PES corresponding to the incidence angle of 20°, where the deeper minimum of $-61.4 \cdot 10^3$ cm^{-1} is observed, on the contrary, at $R_{\text{Cs-Rb}} = 4.1$ Å. However, as for the previous case, in order to arrive at this potential minimum, a barrier of $26.3 \cdot 10^3$ cm^{-1} must be overcome first.

The potential energy surface corresponding to the incidence angle of 30° starts exhibiting the behavior typical of all higher incidence angles for which one potential minimum is observed in the region where all three internuclear distances remain in the region of typical equilibrium states for alkali metal dimers. The features described above are observed for all examined states. Excluding, now, small incidence angles of 10° and 20° as special cases, only angles from 30° to 180° shall be considered further.

Let us examine, now, the topological features of the the PESs relative to each other at different incidence angles Figure 3 shows the PESs of the Rb atom approaching the RbCs dimer from the Rb side (the Rb+RbCs case) at three different incidence angles. At $\theta_{\mathrm{Rb}} = 180°$, the highest degree of degeneracy is observed: all the A$''$ symmetry states coincide with one of the A$'$ symmetry states of the corresponding multiplicity. In particular, $(1)^2\mathrm{A}''$ coincides with $(3)^2\mathrm{A}'$, except in the region where the latter exhibits

Table 3. Spectroscopic constants $R^{\mathrm{A}}_{\min}$ (Å), D^{A}_e (cm^{-1}) for the triatomic $\mathrm{Rb_2Cs}$ system at some incidence angles $\theta^{\mathrm{A}}_{\min}$ of A = Rb, Cs in the RbCs dimer attacked by the third Rb atom. T_e is the energy at the dissociation limit corresponding to the Rb+RbCs or RbCs+Rb systems with constant internuclear distance R_e in the RbCs dimer. The chosen incidence angles correspond either to the minimum on the PES or to a saddle point with respect to the incidence angle (marked with *)

$R_e^{a^3\Sigma^+} = 6.219$ Å															
State	T_e, cm^{-1}	$\theta^{\mathrm{Rb}}_{\min}$, deg	$R^{\mathrm{Rb}}_{\min}$, Å	D^{Rb}_e, cm^{-1}	$\theta^{Cs}_{\min}$, deg	$R^{\mathrm{Cs}}_{\min}$, Å	D^{Cs}_e cm^{-1}	State	T_e, cm^{-1}	$\theta^{\mathrm{Rb}}_{\min}$, deg	$R^{\mathrm{Rb}}_{\min}$, Å	D^{Rb}_e, cm^{-1}	$\theta^{\mathrm{Cs}}_{\min}$, deg	$R^{\mathrm{Cs}}_{\min}$, Å	D^{Cs}_e cm^{-1}
$(1)^2\mathrm{A}'$	0	50	4.28	4359	40	4.60	4244	$(1)^2\mathrm{A}''$	9884	50	4.24	7816	40	4.47	7812
		180*	4.16	3232	180*	4.37	3043			180*	4.14	3718	170*	4.29	4042
$(2)^2\mathrm{A}'$	1204	50	4.81	2833	50	5.20	2942						180	4.29	4044
		110*	5.43	1047	100*	5.60	1059	$(2)^2\mathrm{A}''$	12141	50	4.28	6416	40	4.50	6346
		180	5.40	1097	180	5.55	1135			180*	4.23	4498	180*	4.61	3906
$(3)^2\mathrm{A}'$	8570	50	4.39	6797	50	4.45	6799	$(1)^4\mathrm{A}'$	1204	60	5.46	853	60	5.60	810
		180*	4.54	3349	180*	5.01	3063			150	5.95	285	140*	6.14	290
$(4)^2\mathrm{A}'$	9880	50	4.78	6530	50	4.99	6535			180*	5.95	286	180	6.14	291
		180*	4.12	3721	130*	4.58	3789	$(2)^4\mathrm{A}'$	9880	30	8.40	4098	40*	4.69	3295
					180	4.45	3985			60*	4.12	3188	100	4.33	4095
$(5)^2\mathrm{A}'$	10660	50	4.71	5528	50	5.05	5521			120	4.17	3597	180*	4.31	3899
		180*	5.10	3038	140*	5.08	3103			180*	4.17	3543			
					180	5.27	3169	$(3)^4\mathrm{A}'$	10660	50	4.91	2129	40*	5.12	1254
$(6)^2\mathrm{A}'$	11040	50	4.62	4219	50	4.91	4164			70*	5.80	1333	50	5.03	2138
		100*	4.82	2426	100*	4.90	2048			120	5.25	1857	70*	5.61	1583
		180	4.61	3215	180	4.62	2808			180*	5.24	1754	100	5.47	1901
													180*	5.49	1701
								$(1)^4\mathrm{A}''$	9884	50	4.32	5072	50	4.39	5091
										180*	4.16	3539	170*	4.32	3901
													180	4.32	3902

an avoided crossing with $(4)^2\mathrm{A}'$, where $(1)^2\mathrm{A}''$ and $(4)^2\mathrm{A}'$ coincide. Similarly, $(2)^2\mathrm{A}''$ coincides with $(5-7)^2\mathrm{A}'$, and $(3)^2\mathrm{A}''$ coincides with $(7-9)^2\mathrm{A}'$ in different regions $R_{\text{Rb-Rb}}$ (Figure 3, *a*). The same picture is observed for quartet states: before the avoided crossing between $(1)^4\mathrm{A}'$ and $(2)^4\mathrm{A}'$, $(1)^4\mathrm{A}''$ coincides with the former state, and after the avoided crossing — it coincides with the latter one.

When the incidence angle is 90°, all above-mentioned degeneracies are removed which is clearly seen in Figure 3, *b*. Note also that many avoided crossings also either disappear or are shifted. For example, $(1)^4\mathrm{A}'$ and $(2)^4\mathrm{A}'$ don't exhibit an avoided crossing at all, and the same goes for $(3)^2\mathrm{A}'$ and $(4)^2\mathrm{A}'$. Looking at the incidence angle of 60°, the reverse can be seen; an increase in the number of avoided crossings. Particular focus should be put on the double avoided crossing of the ground state $(1)^2\mathrm{A}'$ with the next highest state in energy of the same $(2)^2\mathrm{A}'$ symmetry, one of which occurs near the equilibrium position of both states. This means that even the lowest in energy ground state of the $\mathrm{Rb_2Cs}$ trimer cannot be considered without accounting for nonadiabatic intramolecular interactions.

Let's now consider the obtained potential energy surfaces. Figure 4 shows that results for the ground $(1)^2\mathrm{A}'$ state for the cases (*a*) Rb+RbCs and (*b*) RbCs+Rb, when the distance in the RbCs dimer is fixed and equal to the equilibrium distance of the dimer in the $\mathrm{X}^1\Sigma^+$ state at 4.427 Å. The curves shown in the diagrams on top correspond to cross-sections with constant incidence angle (i.e. along the horizontal axis of the surfaces shown in the figures on the bottom). Note that, for the doublet ground state $(1)^2\mathrm{A}'$ the equilibrium geometry corresponded to $R_e = 4.543$ Å, $R_{\text{Rb-Rb}} = 5.232$ Å, $\theta_{\mathrm{Cs}} = 70.3°$, and the $\mathrm{Rb_2Cs}$ molecule actually has the lowest energy for (*b*) at an incidence angle of 70°. This topology of the PES is typical for this molecule: for the majority of states, a boomerang-like well is observed and can be clearly seen on these graphs. The vertical portion is always near $R_{\text{A-Rb}} = R_e$ (marked with a vertical white line in the diagrams), the boomerang's corner is within 60°–80°, then a downward sloping tail is observed close to 8 Å at 30°. The latter is associated with the characteristic equilibrium internuclear distances that are observed in alkali metal dimers as mentioned above. Table 2 shows the PES minima and well depth positions with respect to the first dissociation limit for those curves that have a local or global minimum or represent a saddle point with respect to the incidence angle.

Table 2–5 shows the well depths, equilibrium distances and dissociation limits for individual cross-sections. Note that deep (deeper than 5000 cm^{-1}) wells are observed for half of states. At the same time, for $(3)^2\mathrm{A}'$, $(4)^2\mathrm{A}'$, $(5)^2\mathrm{A}'$, $(1)^2\mathrm{A}''$, $(2)^2\mathrm{A}''$, such wells are observed at all four values of R_e, that were considered in this work. It can be also seen from the tables that almost for all states the optimum incidence angle does not depend on which of the dimer

Table 4. Equilibrium spectroscopic constants $R^{\mathrm{A}}_{\mathrm{min}}$ (Å), D^{A}_{e} (cm^{-1}) for the triatomic Rb_2Cs system at some incidence angles $\theta^{\mathrm{A}}_{\mathrm{min}}$ of the Rb atom attacking the RbCs dimers' constituent atoms $\mathrm{A} = \mathrm{Rb}, \mathrm{Cs}$. T_e is the PES value at the dissociation limit corresponding to the Rb_2Cs or RbCs+Rb system with the internuclear distance R_eCs fixed in the RbCs dimer. The chosen incidence angles correspond either to the minimum on the PES or to a saddle point with respect to the incidence angle (marked with *)

$R_e^{b^3\Pi} = 4.314$ Å																
State	T_e, cm^{-1}	$\theta^{\mathrm{Rb}}_{\mathrm{min}}$, deg	$R^{\mathrm{Rb}}_{\mathrm{min}}$, Å	D^{Rb}_{e}, cm^{-1}	$\theta^{\mathrm{Cs}}_{\mathrm{min}}$, deg	$R^{\mathrm{Cs}}_{\mathrm{min}}$, Å	D^{Cs}_{e}, cm^{-1}	State	T_e, cm^{-1}	$\theta^{\mathrm{Rb}}_{\mathrm{min}}$, deg	$R^{\mathrm{Rb}}_{\mathrm{min}}$, Å	D^{Rb}_{e}, cm^{-1}	$\theta^{\mathrm{Cs}}_{\mathrm{min}}$, deg	$R^{\mathrm{Cs}}_{\mathrm{min}}$, Å	D^{Cs}_{e}, cm^{-1}
$(1)^2\mathrm{A}'$	0	60	5.05	1969	50	5.65	1882	$(1)^2\mathrm{A}''$	9065	60	4.29	6494	60	4.40	6500
		70*	4.68	1863	60*	5.06	1870			180*	4.15	2342	180*	4.38	1831
		80	4.41	1884	70	4.62	1984	$(2)^2\mathrm{A}''$	12748	60	4.81	5161	70	4.45	5174
		180*	4.32	1378	180*	4.55	1251			180*	4.24	4025	130*	4.41	4401
$(2)^2\mathrm{A}'$	5097	40*	7.33	2510	30*	7.90	2539						180	4.39	4456
		70	4.24	5693	60	4.58	5824	$(1)^4\mathrm{A}'$	5097	70	5.02	1462	60	5.39	1450
		120*	4.69	2535	100*	4.87	2510			180*	6.05	313	180*	6.22	319
		180	4.68	2681	180	4.83	2760	$(2)^4\mathrm{A}'$	9063	30	7.85	1462	60*	7.23	533
$(3)^2\mathrm{A}'$	9063	50	5.92	5069	50	6.04	4764			80*	6.39	521	120	4.70	1471
		70*	5.12	4631	60*	5.55	4624			140	4.56	1249	180*	4.82	985
		90	4.49	4804	80	4.64	5050			180*	4.52	1217			
		180*	4.15	2342	180*	4.37	1832	$(3)^4\mathrm{A}'$	14425	60*	5.76	2843	70*	5.23	2836
$(4)^2\mathrm{A}'$	11174	70	4.64	5549	60	5.04	5561			70	5.10	2854	180	4.50	4505
		130*	4.72	3226	130*	4.96	3040			80*	4.91	2848			
		180	4.72	3623	180	5.10	3298			180	4.48	2988			
$(5)^2\mathrm{A}'$	12744	40*	6.21	4233	30	7.71	4629	$(1)^4\mathrm{A}''$	9065	60	5.06	2158	70	4.60	2197
		70	4.31	5988	40*	6.99	4540			180*	4.52	1217	180*	4.83	985
		100*	4.60	4535	60	4.63	6110								
		130	4.38	4651	100*	4.82	4179								
		180*	4.25	4025	180	4.48	4434								
$(6)^2\mathrm{A}'$	12748	40*	7.71	1261	30*	8.19	1374								
		70	4.81	3482	60	5.26	3480								
		120*	4.77	1309	100*	4.88	1251								
		180	5.02	2263	180	5.35	2112								

atoms the Rb atom approaches — the optimum incidence angle remains within $50°-80°$ or is close to the angles obtained during geometry optimization. In all cases (for example, for $(3)^2\mathrm{A}'$) when a difference between (a) and (b) is observed, two minima are observed for a particular state, and the former or the latter will be local or global depending on which of the dimer atoms is attacked.

Numerous avoided crossing were also reported before. Let's consider the way they look like on the PES and on cross-sections for $(3)^4\mathrm{A}'$ at different values of R_e (Figure 5). This state exhibits an avoided crossing with $(4)^4\mathrm{A}'$ at $R_{\text{Cs-Rb}} \approx 6$ Å, where an inflection point can be seen on the top graph in Figure 5. It can be also seen that, when the incidence angle varies, the point of avoided crossing shifts towards greater internuclear distances. The other graphs in this figure show the PES at other values of R_e (indicated on the graphs). With shorter internuclear distances in the dimer (R_e), the optimum geometry of the Rb_2Cs molecule is linear — this is clearly seen in the second graph from the top, where a deep well occurs with a minimum at $\theta_{Cs} = 180°$ and $R_{\text{Cs-Rb}} = 4.53$ Åand a depth of more than $4000\,\mathrm{cm}^{-1}$. When R_e increases, the distance $R_{\text{Cs-Rb}}$, where the minimum is observed, increases too, which is clearly seen in Figure 5, were the PES minimum region shifts together with the vertical white line. A significant decrease in the well depth and incidence angle, at which the PES minimum occurs, is also observed.

4. Asymptotic behavior of the PES at the dissociation limit and at different values of R_e

As expected, the 3D PES functions corresponding to different equilibrium distances R_e converge to different dissociation limits, which can be clearly seen by comparing the values of T_e listed in Table 2–5. These values of T_e should correspond at the dissociation limit to the Rb+RbCs system where the internuclear distance is equal to R_e. Figure 6 shows the potential energy curves of the RbCs molecule, vertical lines in the figure mark the equilibrium positions and their length is equal to the Rb atom excitation energy from the ground state to the first excited state $5p$.

Note, here, the typical behavior patterns of pair interatomic potentials of the alkali metal dimers: the $b^3\Pi$ and $X^1\Sigma^+$ states have very close equilibrium positions; inter-

Table 5. Spectroscopic constants $R^{\mathrm{A}}_{\mathrm{min}}$ (in Å), D^{A}_{e} (cm^{-1}) for the triatomic $\mathrm{Rb_2Cs}$ system at some incidence angles of the third Rb atom attacking the RbCs dimer's constituent $\theta^{\mathrm{A}}_{\mathrm{min}}$ $\mathrm{A} = \mathrm{Rb}, \mathrm{Cs}$ atoms. T_e is the value of the PES at the dissociation limit corresponding to the Rb+RbCs or RbCs+Rb systems with constant internuclear distance R_e in the RbCs dimer. The chosen incidence angles correspond either to the minimum value on PES or to a saddle point with respect to the incidence angle (marked with *)

$R_e^{A^1\Sigma^+} = 5.122$Å															
State	T_e, cm^{-1}	$\theta^{\mathrm{Rb}}_{\mathrm{min}}$, deg	$R^{\mathrm{Rb}}_{\mathrm{min}}$, Å	D^{Rb}_{e}, cm^{-1}	$\theta^{\mathrm{Cs}}_{\mathrm{min}}$, deg	$R^{\mathrm{Cs}}_{\mathrm{min}}$, Å	D^{Cs}_{e} cm^{-1}	State	T_e, cm^{-1}	$\theta^{\mathrm{Rb}}_{\mathrm{min}}$, deg	$R^{\mathrm{Rb}}_{\mathrm{min}}$, Å	D^{Rb}_{e}, cm^{-1}	$\theta^{\mathrm{Cs}}_{\mathrm{min}}$, deg	$R^{\mathrm{Cs}}_{\mathrm{min}}$, Å	D^{Cs}_{e} cm^{-1}
$(1)^2\mathrm{A}'$	0	50	5.13	2614	60	4.40	2640	$(1)^2\mathrm{A}''$	9263	60	4.16	6982	50	4.52	7043
		180*	4.22	2013	180*	4.44	1826			180*	4.15	2609	180∗	4.29	2420
$(2)^2\mathrm{A}'$	3245	40*	7.81	1931	50	4.98	4785	$(2)^2\mathrm{A}''$	12746	50	4.85	5659	60	4.33	5686
		60	4.64	5099	110*	5.09	1931			180*	4.27	4567	150*	4.58	4645
		110*	4.89	1933	180	5.04	2155						180	4.59	4655
		180	4.89	2076				$(1)^4\mathrm{A}'$	3245	60	5.31	1192	60	5.38	1211
$(3)^2\mathrm{A}'$	9258	50	5.73	5803	40	6.62	5374			170*	6.06	309	160*	6.15	313
		60*	5.38	5140	50*	6.00	5241			180	6.00	310	180	6.15	314
		80	4.43	5403	80	4.46	5799	$(2)^4\mathrm{A}'$	9258	70*	6.95	522	60*	7.46	523
		180*	4.63	3039	180*	5.04	2693			140	4.31	1993	110	4.45	2334
$(4)^2\mathrm{A}'$	9504	60	4.89	5188	60	5.00	5146			180*	4.30	1943	180*	4.42	1922
		130*	4.29	2580	130*	4.58	2233	$(3)^4\mathrm{A}'$	12179	70*	4.94	1758	30	8.66	2256
		180	4.19	2805	180	4.50	2603			110	4.96	2270	60*	5.40	1632
$(5)^2\mathrm{A}'$	12179	40*	7.29	4440	50	5.04	6655			180*	4.63	1706	180	4.76	2768
		60	4.61	6947	90*	4.66	4443	$(1)^4\mathrm{A}''$	9263	50	5.22	2959	70	4.38	2950
		180*	4.26	4009	120	4.86	4546			70*	4.16	2353	180*	4.42	1925
					180*	4.58	4086			80	4.25	2402			
$(6)^2\mathrm{A}'$	12571	40*	7.44	2313	30*	8.67	2542			180*	4.30	1947			
		70	4.31	4241	50	5.58	4191								
		110*	4.85	2415	100*	4.98	2256								
		180	4.98	3788	180	5.31	3648								

section of the $\mathrm{b}^3\Pi$ and $\mathrm{A}^1\Sigma^+$ states near the equilibrium position of the latter is observed; the intrusion (deep well) of the $\mathrm{C}^1\Sigma^+$ state converging to the third dissociation limit into the energy region containing the states converging to the second limit.

Thus, it is expected that some PESs examined in the previous section and obtained at different R_e will converge to the dissociation limits corresponding to different states of the dimer+atom system. Since the state degeneracy should be retained, it can be expected that only the A' states will converge to the limits corresponding to the system where the dimer is in the excited state with the Σ^+ symmetry and the atom is in the ground state. On the other hand, if the dimer at the dissociation limit is in the Π state, then both the A' and A'' states of the trimer converging to this value are expected. If the dimer is in its singlet state —only doublet states will be observed for the triatomic system at the dissociation limit. And if the dimer is in its triplet state, then both doublet and quartet states of the trimer will converge to this dissociation limit. Three doublet states of the trimer should converge to the limit corresponding to the dimer in its ground state and the excited atom $s \rightarrow p$, where two states should have the A' symmetry corresponding to the p-orbitals in the molecular plane, and one A''-state corresponding to the perpendicular p_z-orbital. The described qualitative patterns of the PES are illustrated in Table 6.

The same table shows the calculated asymptotic values of the PES at the dissociation limit and the list of states converging to the corresponding values. The Energies of the RbCs dimer at the corresponding R_e or the Rb atom excitation energy $\mathrm{Rb}(5s) \rightarrow \mathrm{Rb}(5p)$ are compared with them. For $R_e = 4.314$, 4.427, 5.122, 6.219 Å , mean differences between the values for the trimer and the values for the dimer+atom system is 51, 44, 40 and 34 cm^{-1}. The minimum deviation is observed for all R_e for the dissociation limit corresponding to the Rb atom excitation $\mathrm{Rb}(5s) \rightarrow \mathrm{Rb}(5p)$ with the dimer in its ground state, where the maximum deviation is only 7 cm^{-1} for $R_e = 5.122$ Å. The maximum deviation for all R_e is observed for the states that converge to the $\mathrm{B}^1\Pi+\mathrm{Rb}(5s)$ and $\mathrm{b}^3\Pi+\mathrm{Rb}(5s)$ limits and where results for the trimer exceed the values obtained for the dimer+atom system by 164 and 104, 159 and 96, 142 and 98, 101 and 97 cm^{-1}, respectively. The obtained deviations are typical of the systems consisting of alkali metal atoms. The previous works [24–26,35] that conducted similar calculations of diatomic alkali metal molecules show that such nonrelativistic potential energy calculations (even before the curves are adjusted by accounting for the spin-orbit interaction) yield an error not greater than the vibra-

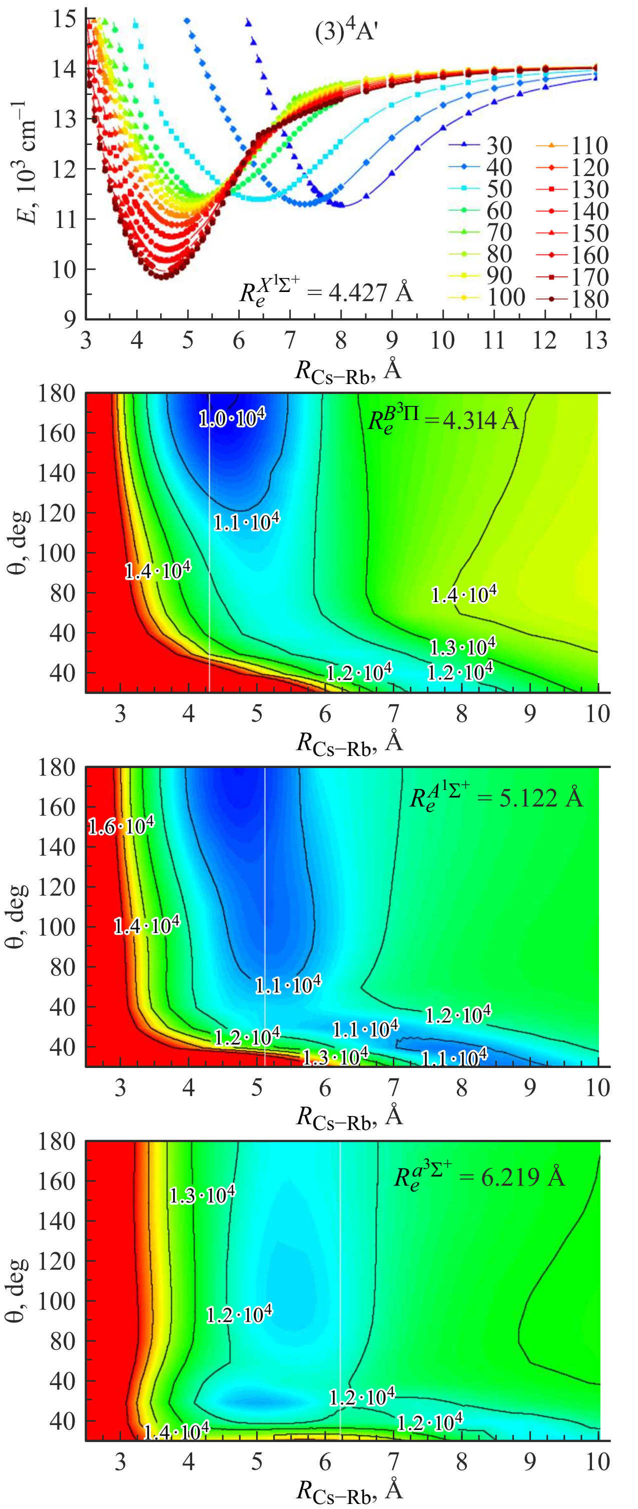

Figure 5. PES of the $(3)^4$A$'$ state of the Rb_2Cs trimer in the RbCs+Rb case at different R_e corresponding to the equilibrium distances in the RbCs dimer in the $X^1\Sigma^+$, $b^3\Pi$, $A^1\Sigma^+$, $a^3\Sigma^+$ states (top to bottom). Vertical white lines correspond to positions when the distance between the incident and attacked atoms is equal to R_e. Each outline corresponds to an energy interval of 1000 cm^{-1}. The value to which the $(1)^2$A$'$ state converges at $R_{\mathrm{Cs\text{-}Rb}} \to \infty$ when $R_e = 4.427$ Å is taken as zero energy here.

Table 6. Value of the PES at the dissociation limit $T_e^{\mathrm{Rb_2Cs}}$ obtained for the trimer with respect to the first dissociation limit, and the combined energy of the RbCs dimer and Rb atom $E^{\mathrm{RbCs+Rb}}$, where the Rb atom in the ground state 5s and the dimer in the $X^1\Sigma^+$ state correspond to zero energy

R_e, Å	States of Rb_2Cs	$T_e^{\mathrm{Rb_2Cs}}$, cm^{-1}	$E^{\mathrm{RbCs+Rb}}$, cm^{-1},	States of RbCs+Rb
4.314	$(1)^2$A$'$	0	0	$X^1\Sigma^+$ + Rb(5s)
	$(2)^2$A$'$, $(1)^4$A$'$	5097	5122	$a^3\Sigma^+$+Rb(5s)
	$(3)^2$A$'$, $(2)^4$A$'$, $(1)^2$A$''$, $(1)^4$A$''$	9064	8960	$b^3\Pi$+Rb(5s)
	$(4)^2$A$'$	11174	11141	$A^1\Sigma^+$+Rb(5s)
	$(5)^2$A$'$, $(6)^2$A$'$, $(2)^2$A$''$	12744	12739	$X^1\Sigma^+$+Rb(5p)
	$(7)^2$A$'$, $(3)^2$A$''$	14054	13890	$B^1\Pi$+Rb(5s)
	$(8)^2$A$'$	14326	14294	$C^1\Sigma^+$+Rb(5s)
	$(9)^2$A$'$, $(3)^4$A$'$	14425	14378	$c^3\Sigma^+$+Rb(5s)
4.427	$(1)^2$A$'$	0	0	$X^1\Sigma^+$+Rb(5s)
	$(2)^2$A$'$, $(1)^4$A$'$	4861	4895	$a^3\Sigma^+$+Rb(5s)
	$(3)^2$A$'$, $(2)^4$A$'$, $(1)^2$A$''$, $(1)^4$A$''$	9085	8989	$b^3\Pi$+Rb(5s)
	$(4)^2$A$'$	10903	10889	$A^1\Sigma^+$ +Rb(5s)
	$(5)^2$A$'$, $(6)^2$A$'$, $(2)^2$A$'$	12736	12739	$X^1\Sigma^+$ +Rb(5p)
	$(7)^2$A$'$, $(3)^2$A$''$	13959	13800	$B^1\Pi$+Rb(5s)
	$(8)^2$A$'$, $(3)^4$A$'$	14057	14011	$c^3\Sigma^+$+Rb(5s)
	$(9)^2$A$'$	14098	14065	$C^1\Sigma^+$+Rb(5s)
5.122	$(1)^2$A$'$	0	0	$X^1\Sigma^+$+Rb(5s)
	$(2)^2$A$'$, $(1)^4$A$'$	3245	3301	$a^3\Sigma^+$+Rb(5s)
	$(3)^2$A$'$, $(2)^4$A$'$, $(1)^2$A$''$, $(1)^4$A$''$	9258	9160	$b^3\Pi$+Rb(5s)
	$(4)^2$A$'$	9504	9481	$A^1\Sigma^+$+Rb(5s)
	$(5)^2$A$'$, $(3)^4$ A$'$	12179	12138	$c^3\Sigma^+$+Rb(5s)
	$(6)^2$A$'$	12571	12546	$C^1\Sigma^+$+Rb(5s)
	$(7)^2$A$'$, $(8)^2$A$'$, $(2)^2$A$''$	12746	12739	$X^1\Sigma^+$+Rb(5p)
	$(9)^2$A$'$, $(3)^2$A$''$	13292	13150	$B^1\Pi$+Rb(5s)
6.219	$(1)^2$A$'$	0	0	$X^1\Sigma^+$+Rb(5s)
	$(2)^2$A$'$, $(1)^4$A$'$	1204	1255	$a^3\Sigma^+$+Rb(5s)
	$(3)^2$A$'$	8570	8570	$A^1\Sigma^+$+Rb(5s)
	$(4)^2$A$'$, $(2)^4$A$'$, $(1)^2$A$''$, $(1)^4$A$''$	9880	9783	$b^3\Pi$+Rb(5s)
	$(5)^2$A$'$, $(3)^4$A$''$	10660	10610	$c^3\Sigma^+$+Rb(5s)
	$(6)^2$A$'$	11040	11005	$C^1\Sigma^+$+Rb(5s)
	$(7)^2$A$''$, $(2)^2$A$''$	12141	12040	$B^1\Pi$+Rb(5s)
	$(8)^2$A$'$, $(9)^2$A$'$, $(3)^2$A$''$	12747	12739	$X^1\Sigma^+$+Rb(5p)

tional quantum of the corresponding state despite the fact that the spin-orbit interaction in the molecules containing the Cs and Rb atoms is quite significant. The spin-orbit interaction must obviously be corrected for to ensure a more accurate description of states of this system, however, since no experimental data for this system are available yet, it has been decided not to conduct a nonadiabatic analysis

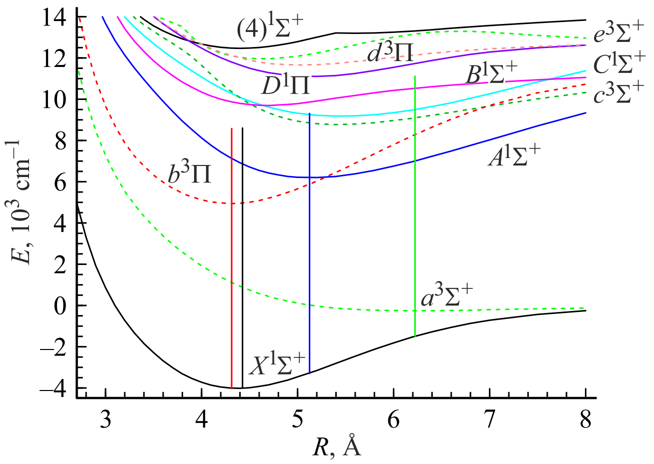

Figure 6. Potential energy curves for the RbCs dimer depending on the internuclear distance. Left to right, the vertical lines mark the equilibrium state positions $R_e = 4.314$, 4.427, 5.122, 6.219 Å of the minima of the $b^3\Pi$, $X^1\Sigma^+$, $A^1\Sigma^+$ and $a^3\Sigma^+$ states, respectively. The vertical line length correspond to the Rb atom excitation energy Rb(5s) →Rb(5p) in 12739 cm^{-1} [31].

of states within the scope of this study. Table 6 also makes it possible to determine the approximate order of accuracy of the obtained PESs. As mentioned above, the maximum deviation of the asymptotic value for the trimer in the dimer + atom limit from the direct dimer calculations equal to 164 cm^{-1}, which is comparable with the mean errors of 50−100 cm^{-1} observed in the potential energy curve calculation for alkali metal dimers with respect to experiment [24,35]. As a result, it can be expected that the mean error of the obtained surfaces is at most 100 cm^{-1} and the error of the geometrical parameters will be approx. 0.02 – 0.05 Å.

Figure 6, as well as Table 6, clearly shows that at different values of R_e different dissociation limit orders are observed in accordance with the electronic level orders in the RbCs dimer at different internuclear distances. For example, when looking at the vertical cross-section in Figure 6 at the internuclear distance of 5.122 Å corresponding to the equilibrium distance of the RbCs dimer in its $A^1\Sigma^+$ state, it can be seen that the trimer will have three dissociation limits lying approximately at 12500 cm^{-1}: two of them will correspond to the excited dimer (in the $c^3\Sigma^+$ and $C^1\Sigma^+$ states) + ground-state atom combination, and one dissociation limit will correspond to the ground-state dimer + excited 5p-state Rb atom combination. It is important to note here: that the $C^1\Sigma^+$ state at the dissociation limit of three isolated atoms converges to Rb(5s) + Rb(5s) + Cs(6p) unlike other levels that converge to the dissociation limit Rb(5p) + Rb(5s) + Cs(6s). This means that, to describe the behavior of the PES of the excited trimer states correctly, states converging to the second and third dissociation limits cannot be considered in isolation, on the contrary, they must be described simultaneously.

5. Conclusion

Ab initio quantum chemical calculations of the electronic structure for the ground state and some excited doublet and quartet states of the heteronuclear Rb_2Cs molecule have provided the 3D potential energy surfaces of the Rb atom approaching the RbCs dimer both towards the Cs atom and towards the Rb atom at different incidence angles varying from 10° to 180°. It has been found that the $(1)^2A'$ electronic ground state of the Rb_2Cs molecule exhibited avoided crossings with the first excited $(2)^2A'$ state in the vicinity of the equilibrium geometry of the first state, consequently the ground state of this trimer cannot be described within the common adiabatic approximation. For all 12 studied states, equilibrium geometries have been determined and appear to belong to the symmetry point group C_{2v}. For all geometries, except the linear one, the equilibrium geometry was found to be an isosceles triangle geometry, where the distances between the Cs atom and each of the Rb atoms coincide.

The PESs obtained in this study may be used for rigorous quantum calculation of collision cross-sections (depending on the energy level) and reaction rate constants for reactions between the RbCs dimer and Rb atom. As noted above, these reactions are one of the root cause of concentration loss (breakdown) of alkali metal dimers in the corresponding Bose−Einstein atomic-molecular condensate. The calculated PESs may be used in future precision analysis of the rovibronic structure of the Rb_2Cs trimer by solving the 3D-vibrational-rotational Schrödinger equation. The rovibronic energies and wave functions obtained from numerical calculation may be used (together with the calculated eigen state dipole moment surfaces, electronic transition dipole moments, and nonadiabatic spin-orbital matrix elements) to forecast optimum routes of optical synthesis and cooling of the Rb_2Cs molecules.

Funding

This study was supported by grant № 22-73-00095 provided by the Russian Science Foundation , https://rscf.ru/project/22-73-00095/.

Conflict of interest

The authors declare that they have no conflict of interest.

References

[1] B.R. Heazlewood, T.P. Softley. Nat. Rev. Chem., **5**, 125−140 (2021). DOI: 10.1038/s41570-020-00239-0

[2] M.G. Hu, Y. Liu, M.A. Nichols, L. Zhu, G. Quéméner, O. Dulieu, K.K. Ni. Nat. Chem., **13** (May), 435−440 (2021). DOI: 10.1038/s41557-020-00610-0

[3] M. Gacesa, J.N. Byrd, J. Smucker, J.A. Montgomery, R. Côté. Phys. Rev. Res., **3** (2), 1−14 (2021). DOI: 10.1103/PhysRevResearch.3.023163

[4] R. Sawant, J.A. Blackmore, P.D. Gregory, J. Mur-petit, D. Jaksch, J. Aldegunde, J.M. Hutson, M.R. Tarbutt, S.L. Cornish. New J. Phys., **22**, 013027 (2020). DOI: 10.1088/1367-2630/ab60f4

[5] A. Kruckenhauser, L.M. Sieberer, L. De Marco, J.R. Li, K. Matsuda, W.G. Tobias, G. Valtolina, J. Ye, A.M. Rey, M.A. Baranov, P. Zoller. Phys. Rev. A, **102** (2), 1−19 (2020). DOI: 10.1103/PhysRevA.102.023320

[6] J. Klos, H. Li, E. Tiesinga, S. Kotochigova. New J. Phys., **24** (2), 025005 (2022). DOI: 10.1088/1367-2630/ac50ea

[7] M. Karra, K. Sharma, B. Friedrich, S. Kais, D.R. Herschbach. J. Chem. Phys., **144** (9) (2016). DOI: 10.1063/1.4942928

[8] P.D. Gregory, J.A. Blackmore, F.M. D, L.M. Fernley, S.L. Bromley, J.M. Hutson, S.L. Cornish. New J. Phys., **23** (12), 125004 (2021). DOI: 10.1088/1367-2630/ac3c63

[9] B. Zhu, B. Gadway, J. Schachenmayer, M.L. Wall, K.R.A. Hazzard, B. Yan, S.A. Moses, J.P. Covey, D.S. Jin, J. Ye, M. Holland, A.M. Rey. Phys. Rev. Lett., **112**, 070404 (2014). DOI: 10.1103/PhysRevLett.112.070404

[10] L. Anderegg, S. Burchesky, Y. Bao, S.S. Yu, T. Karman, E. Chae, K.K. Ni, W. Ketterle, J.M. Doyle. Science, 373 (August), 779-782 (2021). DOI: 10.1126/science.abg9502

[11] E.A. Pazyuk, A.V. Zaitsevskii, A.V. Stolyarov, M. Tamanis, R. Ferber. Rus. Chem. Rev., **84** (10), 1001−1020 (2015). DOI: 10.1070/RCR4534

[12] T.A. Isaev. Physics Uspekhi, **190** (03), 313−328 (2020). DOI: 10.3367/ufnr.2018.12.038509

[13] L. Kranabetter, H.H. Kristensen, C.A. Schouder, H. Stapelfeldt. J. Chem. Phys., **160** (13), 1−7 (2024). DOI: 10.1063/5.0200389

[14] J. Schnabel, T. Kampschulte, S. Rupp, J.H. Denschlag, A. Köhn. Phys. Rev. A, **103** (2), 022820 (2021). DOI: 10.1103/PhysRevA.103.022820

[15] P. Jasik, J. Kozicki, T. Kilich, J.E. Sienkiewicz, N.E. Henriksen. Phys. Chem. Chem. Phys., **20** (27), 18663−18670 (2018). DOI: 10.1039/c8cp02551g

[16] M.D. Frye, J.M. Hutson. New J. of Phys., **23** (12) (2021). DOI: 10.1088/1367-2630/ac3ff8

[17] H. Jing, J. Cheng, P. Meystre. Phys. Rev. A, **77** (4), 1−8 (2008). DOI: 10.1103/PhysRevA.77.043614

[18] V. Olaya, J. P.erez-Ríos, F. Herrera. Phys. Rev. A, **101** (3), 1−12 (2020). DOI: 10.1103/PhysRevA.101.032705

[19] M. Śmiałkowski, M. Tomza. Phys. Rev. A, **101** (1) (2020). DOI: 10.1103/PhysRevA.101.012501

[20] P. Soldán. Phys. Rev. A, **82** (3), (2010). DOI: 10.1103/PhysRevA.82.034701

[21] T.V. Tscherbul, G. Barinovs, J. Kłos, R.V. Krems. Phys. Rev. A, **78**, 022705 (2008). DOI: 10.1103/PhysRevA.78.022705

[22] P.S. Zuchowski, J.M. Hutson. Phys. Rev. A, **81** (6), 060703 (2010). DOI: 10.1103/PhysRevA.81.060703

[23] M. Tomza, K.W. Madison, R. Moszynski, R.V. Krems. Phys. Rev. A, **88**, 050701(R) (2013). DOI: 10.1103/PhysRevA.88.050701

[24] E.A. Bormotova, S.V. Kozlov, E.A. Pazyuk, A.V. Stolyarov, W. Skomorowski, I. Majewska, R. Moszynski. Phys. Rev. A, **99** (1), 12507 (2019). DOI: 10.1103/PhysRevA.99.012507

[25] E.A. Bormotova, S.V. Kozlov, E.A. Pazyuk, A.V. Stolyarov. Phys. Chem. Chem. Phys., **20** (3), 1889−1896 (2018). DOI: 10.1039/C7CP05548J

[26] E.A. Bormotova, S.V. Kozlov, E.A. Pazyuk, A.V. Stolyarov, I. Majewska, R. Moszynsky. Phys. Chem. Chem. Phys., **23** (9), 5187−5198 (2021). DOI: 10.1039/D0CP06487D

[27] E.A. Bormotova, A.S. Likharev, A.V. Stolyarov. Opt. i spektr., **131** (9), 1163−1172 (2023) (in Russian). DOI: 10.61011/EOS.2024.07.59642.6426-24

[28] I.S. Lim, P. Schwerdtfeger, B. Metz, H. Stoll. J. Chem. Phys., **122** (10), 104103 (2005). DOI: 10.1063/1.1856451

[29] W. Müller, J. Flesch, W. Meyer. J. Chem. Phys., **80**, 3297 (1984). DOI: doi:10.1063/1.447083

[30] A. Zaitsevskii, N.S. Mosyagin, A.V. Stolyarov, E. Eliav. Phys. Rev. A, **96** (2), 1−9 (2017). DOI: 10.1103/PhysRevA.96.022516

[31] A. Kramida, Yu. Ralchenko, J. Reader, and NIST ASD Team. NIST Atomic Spectra Database, NIST, Gaithersburg, MD. (2023). https://physics.nist.gov/asd

[32] H. Werner, P. Knowles, G. Knizia, F. Manby, M. Schütz, P. Celani, T. Korona, R. Lindh, A. Mitrushenkov, G. Rauhut, et al. Molpro, version 2010.1, a package of ab initio programs (2010). http://www.molpro.net

[33] A. Allouche, M. Korek, K. Fakherddin, A. Chaalan, M. Dagher, F. Taher, M. Aubert-Frécon. J. Phys. B, **23**, 2307−2316 (2000). DOI: 10.1088/0953-4075/33/12/312

[34] J. Lozeille, A. Fioretti, C. Gabbanini, Y. Huang, H.K. Pechkis, D. Wang, P.L. Gould, E.E. Eyler, W.C. Stwalley, M. Aymar, O. Dulieu. Eur. Phys. J. D, **39** (2), 261−269 (2006). DOI: 10.1140/epjd/e2006-00084-4

[35] S.V. Kozlov, E.A. Bormotova, A.A. Medvedev, E.A. Pazyuk, A.V. Stolyarov, A. Zaitsevskii. Phys. Chem. Chem. Phys., **22**, 2295−2306 (2020). DOI: 10.1039/C9CP06421D

Translated by EgoTranslating